HOW ACCURATELY CAN WE MEASURE FROM VIDEO? PRACTICAL CONSIDERATIONS AND ENHANCEMENTS OF THE CAMERA CALIBRATION PROCEDURE

Aliaksei Laureshyn
Transport & Roads
Department of Technology & Society
Faculty of Engineering, LTH
Lund University
Box 118
22100 Lund, Sweden
Tel: +46 46 222 31 91 Email: aliaksei.laureshyn@tft.lth.se

Mikael Nilsson
Centre of Mathematical Sciences
Faculty of Engineering, LTH
Lund University
Box 118
22100 Lund, Sweden
Tel: +46 46 222 08 96 Email: micken@maths.lth.se

Word count: 3,700 words text + 15 tables/figures x 250 words (each) = 7,450 words

Submission Date: 14 July 2017

ABSTRACT

The accuracy of position measurements from videos depends greatly on the quality of the camera calibration model parameters. This paper investigates how such factors as camera height and the selection of calibration points affect the quality of the final calibration model. A series of controlled experiments is performed in traffic or similar-to-traffic environments, where the accuracy of measurements from videos is compared to measurements taken with other tools. To enhance the calibration process, a multi-camera approach is suggested that utilises the information about 'common points'—points seen on several cameras but with unknown world co-ordinates. The performed tests show that the calibration quality can greatly benefit from this approach. The paper is addressed primarily to traffic researchers developing own video-based tools for road users observations.

Keywords: Camera calibration, TSAI model, Accuracy, Video analysis

INTRODUCTION

The video recording and extraction of microscopic data, such as road user position and speed, from videos is a commonly used method in many road traffic studies. Examples of such applications include surrogate safety analysis [1-5], behavioural analysis [6, 7] and the calibration of microscopic traffic models [8-10]. A crucial step before objective measurements from a video can be taken is camera calibration, i.e. the definition of a model that relates the position of a point **A** in world co-ordinates (x_w, y_w, z_w) to its representation **a** (x_i, y_i) in the camera image (FIGURE 1).

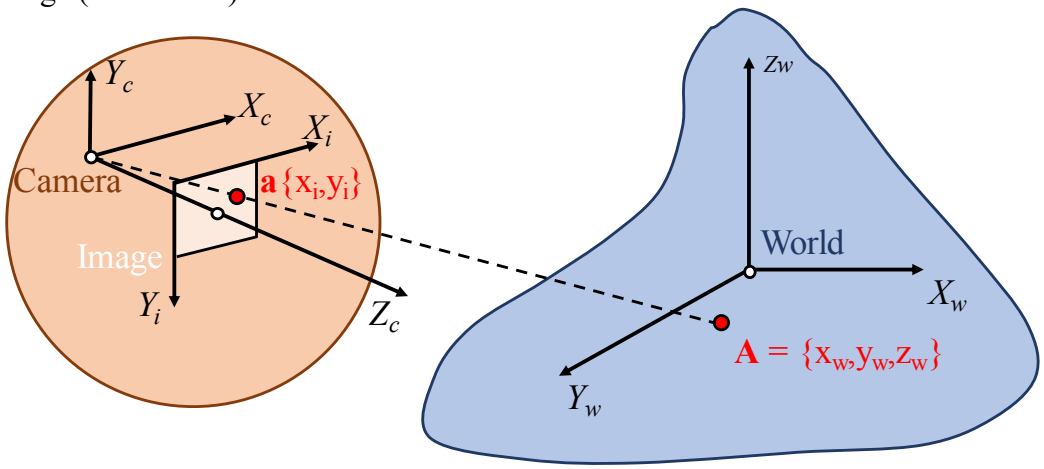

FIGURE 1. Calibration model principle

Several techniques for camera calibration have been suggested, the most common being Tsai (1987), Heikkilä and Silven (1997) and Zhang (2000) [11-13]. This study uses the Tsai calibration model, which incorporates linear equations based on the radial alignment constraint and a second-order radial term that handles lens distortions (the exact mathematical description can be found elsewhere, e.g. [12]).

One important mathematical property of the calibration model deserves mentioning here. Transforming three-dimensional (3D) world coordinates to an image can be done unambiguously, but this is not the case for transforming in the opposite direction (from an image to the world). An image point corresponds to a series of points in the 3D space or, more specifically, all the points along a ray (see the dashed line in FIGURE 1). Therefore, it is necessary to have additional information (usually, the point's *z*-coordinate) to define a single corresponding point in the real world. This problem is often tackled using an approximation that states the part of the road surface visible in an image is a perfect plane, i.e. the *z*-coordinate of the road user footprint is always zero (we will refer to it later as the "zero-plane").

The parameters of the calibration model with a fixed mounted camera are usually estimated based on a set of points with a known position in an image and known world co-ordinates. Once again, we omit the heavy mathematical description of the process that can be found, for example, in [12].

Video-based tools available on the market comes usually with a list of recommendations on how the cameras should be installed [14]. However, a traffic researcher willing to develop own tools with functionality beyond what the 'standrad sensors' have to offer, usually have to find his/her

own way by trials and errors which might often be costly in time, energy and amount of frustration. The purpose of this paper is to provide practical hints and better understanding on which factors affect the quality of the camera calibration model and consequently the measurements taken from a video and the extent of these effects. Several real-world experiments have been conducted testing the different factors, such as camera perspective, location of the points used for calibration, etc. A multi-camera approach is also suggested to enhance the quality of the calibration model.

In this study, we use used a software tool called T-Calibration [15], which is available as a free download. The software is originally written based on the TSAI model description [12] except for the module of the model parameters' initialisation which utilises the code of Reg Willson [16].

WHAT AFFECTS THE ACCURACY OF MEASUREMENTS FROM A VIDEO?

A long list of factors can affect the accuracy of measurements taken from a video. The most important can be listed as:

- Camera height and perspective
- Camera resolution
- The distance from the camera to the studied object (see FIGURE 2)
- The quality of the calibration model

FIGURE 2. The 'size' of one camera image pixel in real-world distance units

An objective measure of the calibration model quality is the descripancy between the actual position of a calibration point in the image and projection to the image of its world co-ordinates (further noted as *e*, measured in pixels) or, alternatively, the actual position of a calibration point in the world and its projection from the image (further noted as *E*, measured in meters) – see FIGURE 3. As the optimisation criteria of the calibration model parameters, minimisation of one of the following parameters can be used:

- $\bar{E}$, *m* – average of the discrepancies between the points in world co-ordinates and their projections from the camera view
- E_{max}, *m* – maximum discrepancy value in world co-ordinates

- $\bar{e}$, *pxl* – average of the discrepancies between the points and their projections from the world in the camera image
- e_{max}, *pxl* – maximum discrepancy value in the camera image

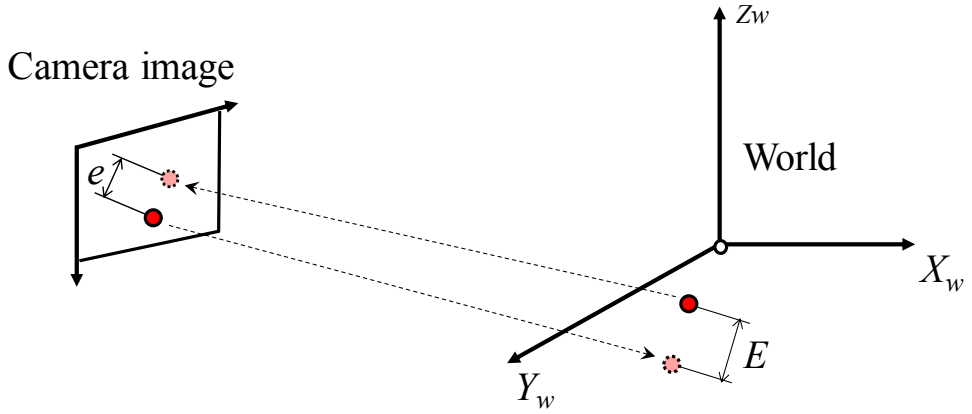

FIGURE 3. Descripancies between the true and 'projected' positions of a calibration point due to imperfections of the calibration model.

However, the final judgement of the obtained calibration model is as much an art as it is a precise science. Low values for *E* and *e* do not necessarily guarantee the calibration model will have a good quality. In practice, the number of available calibration points is usually limited, and these points do not necessarily cover the entire scene as evenly as desired. In this case, the optimisation may 'force' the model to fit the available points well, but for the areas with no points, the calibration quality will still remain uncertain.

At least some initial clues regarding the general model fit can be obtained from a visual check. This can be done by, for example, placing a grid of regularly positioned points in the road plane and projecting them to the camera view. Strange curvatures and distortions (FIGURE 4) would indicate that a further enhancement of the calibration model is necessary.

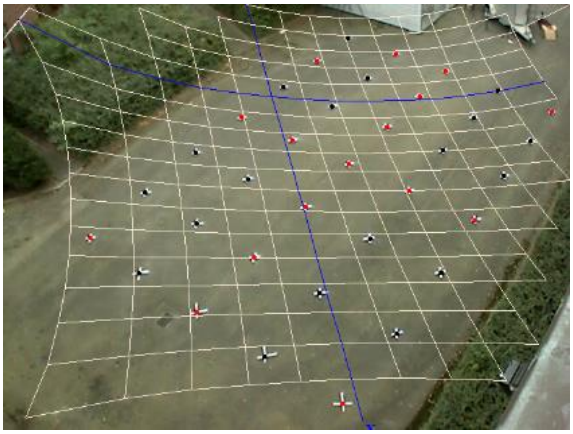

FIGURE 4. The grid placed on the road surface suggests a poor quality of the calibration model, even though the error metrics on the calibration points are low

DATASET I

Data collection set-up

A grid of 35 points (cell size 2 m) was marked on a flat, traffic-free space surrounded by building blocks (FIGURE 5). Cameras 1 and 2 were installed almost exactly above each other on the outdoor emergency ladder (heights 5.5 m and 8 m) and Cameras 3 and 4 on the roof (height 11 m). The points' positions were measured accurately with a theodolite (measurement error <1 cm). The height difference between the individual points did not exceed 1–2 cm, and, despite being considered in all calculations, it did not produce any noticeable effect.

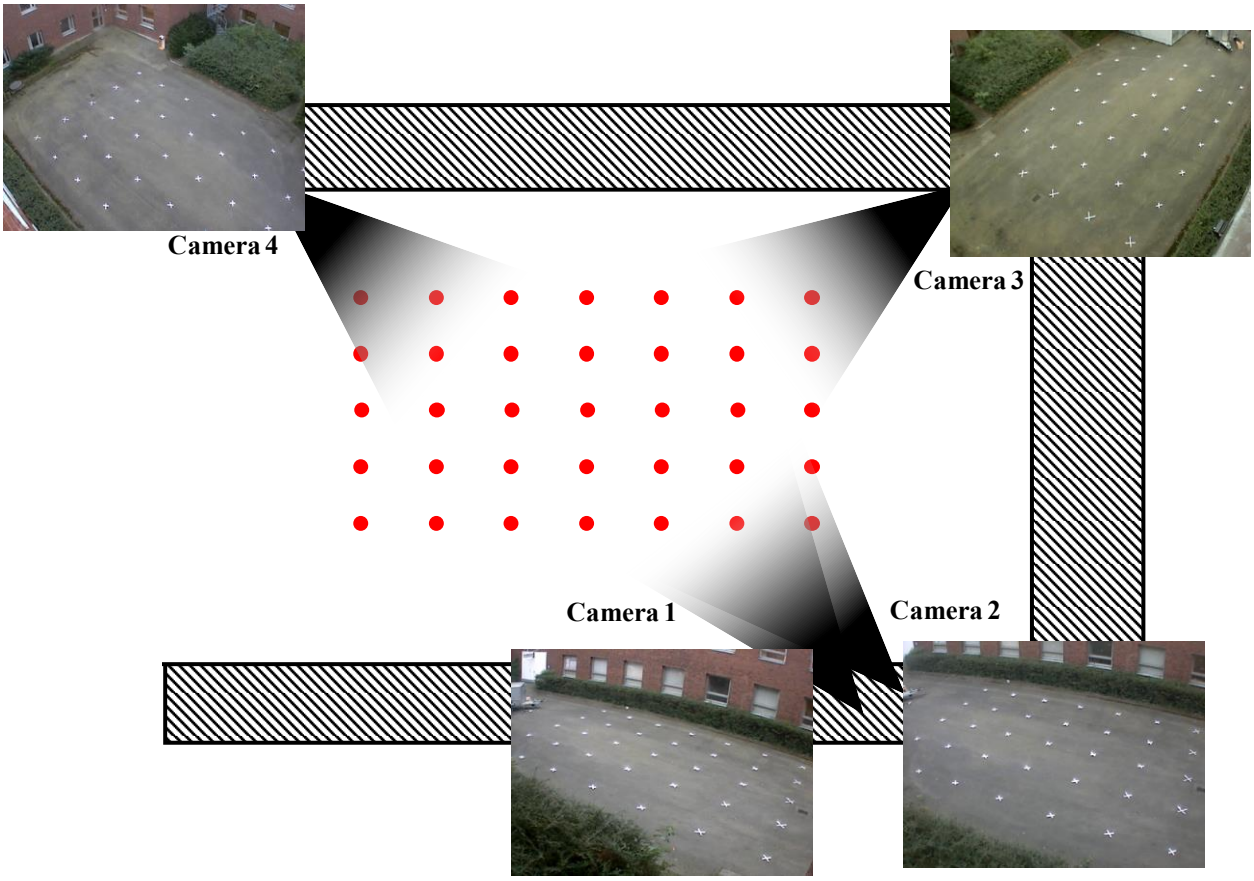

FIGURE 5. Camera set-up for Dataset I

This set-up is much more accurate compared to what is considered "normal" accuracy in traffic studies. In a sense, it is a controlled simulation, close enough to real road environments, but it allows for testing of the effects of different factors, such as the selection of calibration points, camera angle and introduced errors in calibration point co-ordinates.

Experiment 1

The main objective of this experiment was to investigate how the camera angle and the selection of calibration points affect the final calibration model quality. Views from Cameras 1, 2 and 3 were used, as their views of the calibration points were highly similar (though "mirrored" for Camera 3), except for the camera installation heights. The following scenarios were tested (FIGURE 6):

- ***S1***: all the available points used for calibration;

- ***S2***: few points evenly distributed over the outer border of the studied area and no points in the middle; this is a typical situation for an urban intersection where many calibration points can be found at zebra crossings around the intersection, but there are no points in its central part;
- ***S3***: few points concentrated in the corner close to the camera;
- ***S4***: few points in the corner far away from the camera.

The results are presented in FIGURE 6 and TABLE 1. Scenario S1 is the 'perfect case', in which many calibration points are evenly distributed over the entire image. All three camera installations provide excellent accuracy, even though it can be noted that, in full accordance with theory, real-world errors slightly increase as the camera height lowers.

Scenario S2, despite the increase in errors, still appears quite usable, as the points, though not as frequent as in S1, still cover a large area of the image. Adversely, scenarios S3 and S4 clearly demonstrate how the accuracy deteriorates as the measurements are attempted in the image areas that do not have any calibration points in the vicinity. A bit surprisingly (and against what theory would suggest), the increased camera height does result in a systematically improved accuracy from Camera 1 to Camera 3 within these scenarios. It appears the location of the calibration points has a much stronger effect on the overall accuracy compared to what can be gained from the increased camera height.

TABLE 1. Calibration quality parameters for Experiment I

		Camera 1 *5.5 m*	**Camera 2** *8 m*	**Camera 3** *11 m*
S1	Points	34	34	35
	$\bar{E}$, cm	2	1	1
	E_{max}, cm	9	5	3
	$\bar{e}$, pxl	0	0	0
	e_{max}, pxl	1	1	1
S2	Points	6	6	6
	$\bar{E}$, cm	3 (2)	2 (1)	3 (1)
	E_{max}, cm	10 (10)	5 (4)	8 (3)
	$\bar{e}$, pxl	1 (1)	1 (0)	1 (0)
	e_{max}, pxl	3 (1)	2 (2)	2 (1)
S3	Points	5	5	5
	$\bar{E}$, cm	25 (1)	8 (0)	19 (1)
	E_{max}, cm	93 (5)	35 (1)	73 (2)
	$\bar{e}$, pxl	5 (0)	2 (0)	4 (0)
	e_{max}, pxl	19 (2)	5 (0)	9 (1)
S4	Points	5	5	5
	$\bar{E}$, cm	24 (2)	42 (4)	31 (0)
	E_{max}, cm	87 (8)	92 (13)	149 (1)
	$\bar{e}$, pxl	8 (0)	15 (1)	10 (0)
	e_{max}, pxl	28 (1)	54 (2)	47 (0)

Note: For the discrepancies *E* and *e*, the main values in the table are calculated for all the calibration points. Values in brackets are calculated only for the points actually used for calibration.

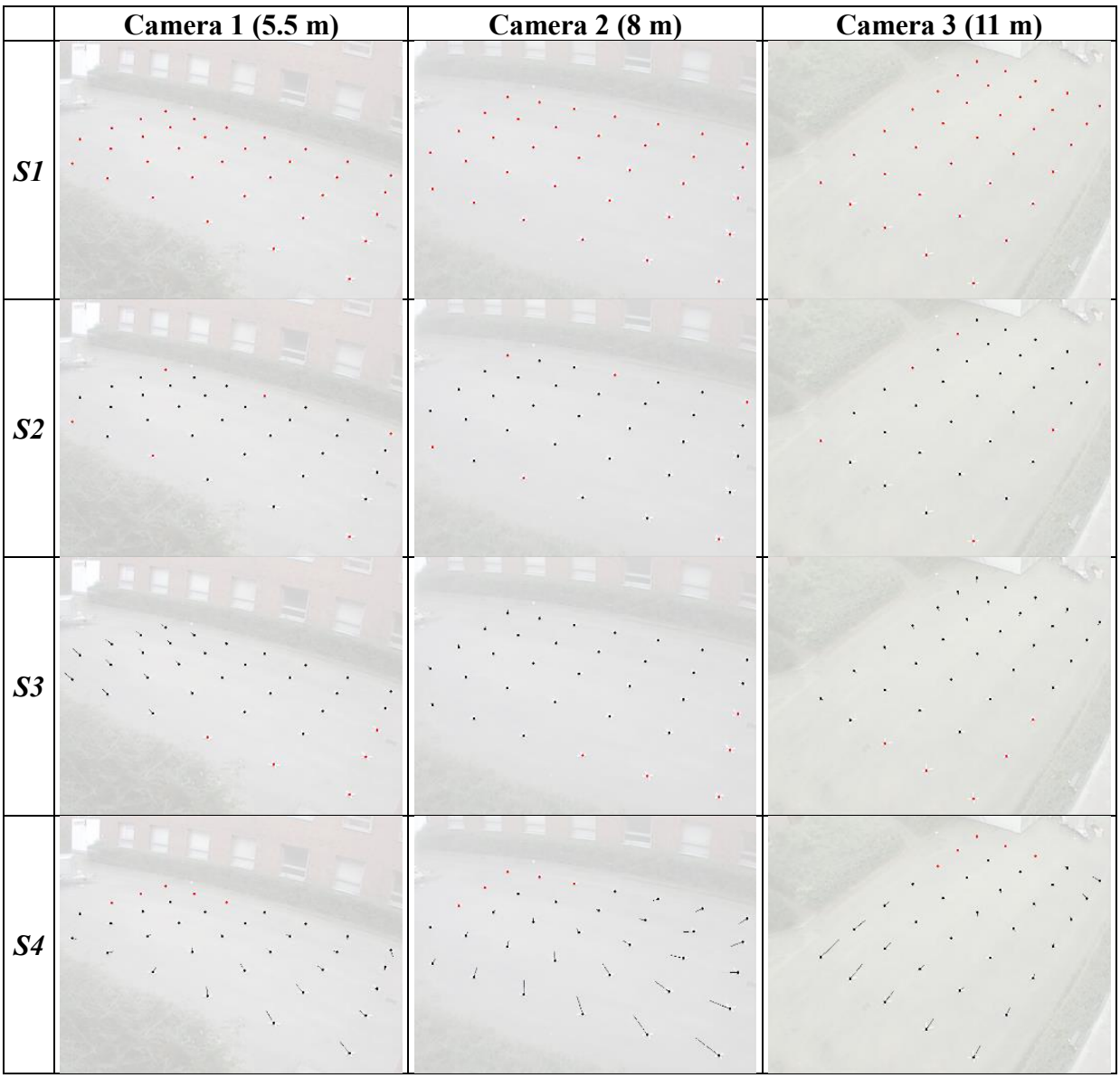

FIGURE 6. Calibration point selection for Experiment I. Points used for calibration are marked **red**. Error vectors connect the points in the image with the projection of the corresponding point from the world co-ordinates. Note how error vectors increase with the distance from the calibration points in scenarios S3 and S4.

Experiment 2

This experiment investigates how the accuracy of the world co-ordinates for the calibration points affects the calibration model's quality. It is common that instead of measuring the points with a theodolite or similar high-accuracy instrument in the field, their positions are extracted from satellite photos provided by such services as Google Earth or Bing Maps. Such photos are often blurry and outdated, and even though they provide a good general overview and indicate where approximately the point should be, the actual position measured is not quite accurate.

In this test, we use the points from scenario S2 in the previous experiment, as it is the most typical situation in the case of traffic videos. The actual world co-ordinates of the calibration

points are modified with added errors *dx* and *dy*, generated randomly from a normal distribution with $\mu = 0$ and chosen σ. The calibration procedure is repeated 100 times with newly generated *dx* and *dy* values, and the final distributions of the calibration errors are presented in FIGURE 7.

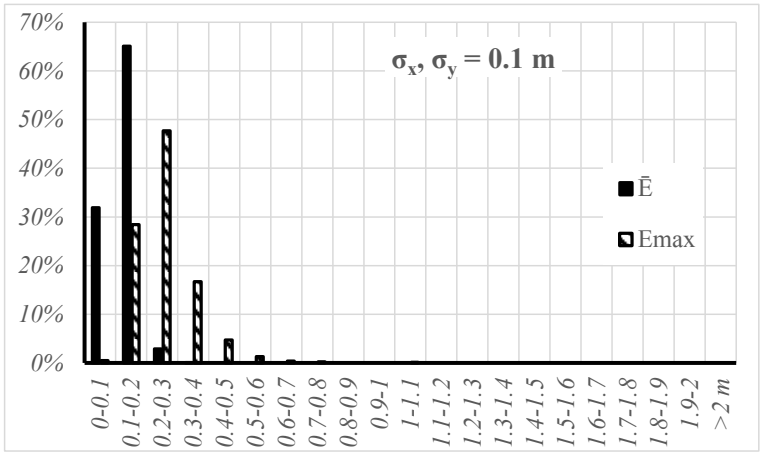

a)

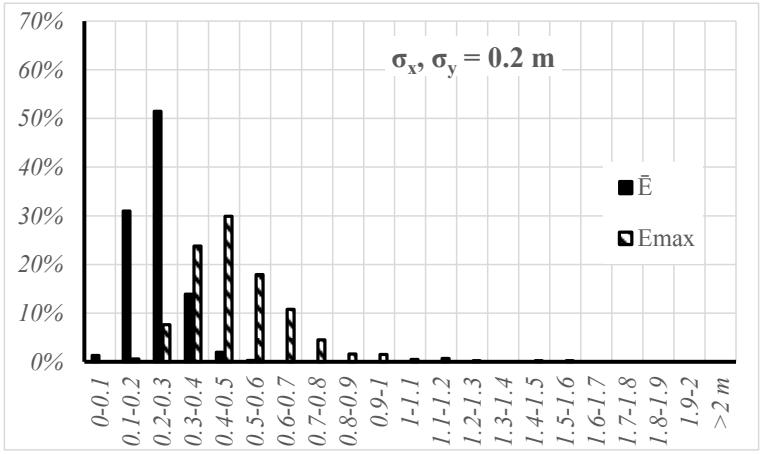

b)

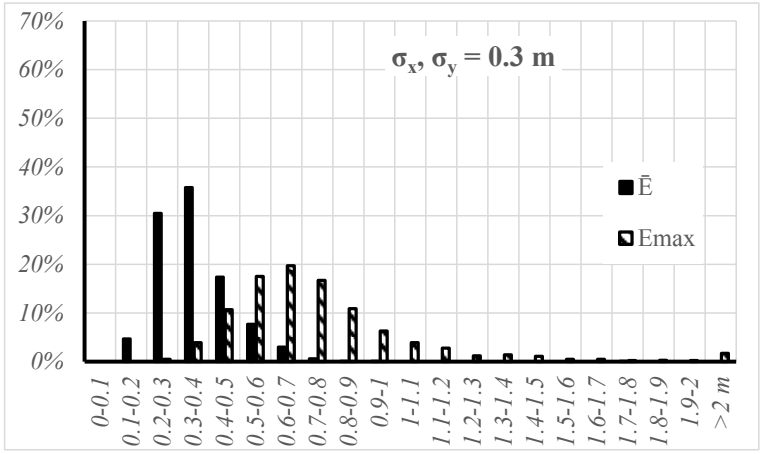

c)

FIGURE 7. Distribution of the calibration $\bar{E}$ and E_{max} for simulated "inaccurate" world co-ordinates of the calibration points.

If the random variables that characterize the population are normally distributed, then there is

approximately a 95 percent probability that the sample mean is within ±2 standard deviations of the population mean (i.e. it can be roughly assumed that σ = 10 cm represents the accuracy of the point measurement ±20 cm). It can be seen from FIGURE 7 that even with a small σ, there are some cases with an E_{max} value up to 80 cm, which is clearly unusable. This indicates how important it is to ensure that the obtained calibration model really makes sense, for example, using a visual check (FIGURE 4). 'Guessing' the position of the points, which are not really seen in the satellite image, is probably not advisable either.

Experiment 3

In this test, we examine whether the use of a multi-camera set-up can improve the calibration quality of each individual camera. It is common that the potential calibration points seen well in the satellite image are not visible in the camera view and vice versa. However, if several camera views are available, points not seen on one camera might be seen on another, etc. Moreover, there are usually many "common" points found in all camera views, but not in the satellite image. Examples of such points can include water traces on asphalt, shadows or the wheel position of a stopped vehicle (given that the camera images are taken at approximately the same time).

The following algorithm for multi-camera calibration is suggested:

1. Each camera is calibrated independently based on "few" points that can be identified in both the satellite image and the camera view.
2. The "common" points are projected to the world co-ordinates using the available calibration models.
3. Because the world co-ordinates of a point suggested by each camera differ, they are "weighed" into a single value in the simplest case by taking an average.
4. Each camera is again calibrated, now using an extended set of points with world co-ordinates.
5. Steps 3 to 5 are repeated until further iterations do not yield any improvements.

To test this approach, we used the views from Cameras 1 and 4. For the initial calibration, a highly limited and unfavourable set of points was selected (FIGURE 8). These were complemented by 10 'common points', marked in each camera but without the real-world co-ordinates. After approximately 10 iterations, no visible changes were produced. The results of the initial individual calibration and final multi-camera calibration are presented in TABLE 2.

TABLE 2. Calibration quality with single- and multi-camera approaches

	Individual calibrations		Multi-set up calibrations	
	Camera 1	**Camera 4**	**Camera 1**	**Camera 4**
$\bar{E}$, cm	20	6	9	7
E_{max}, cm	66	25	24	14
$\bar{e}$, pxl	8	2	3	2
e_{max}, pxl	41	9	9	6

The use of additional calibration points, despite with an estimated and not perfectly accurate real-world position, greatly improved the calibration accuracy, particularly for Camera 1, where both the average and maximum errors greatly decreased. For Camera 4, the average error did not change, but the maximum error also decreased, indicating the calibration became more consistent

over the entire image.

a)

b)

c)

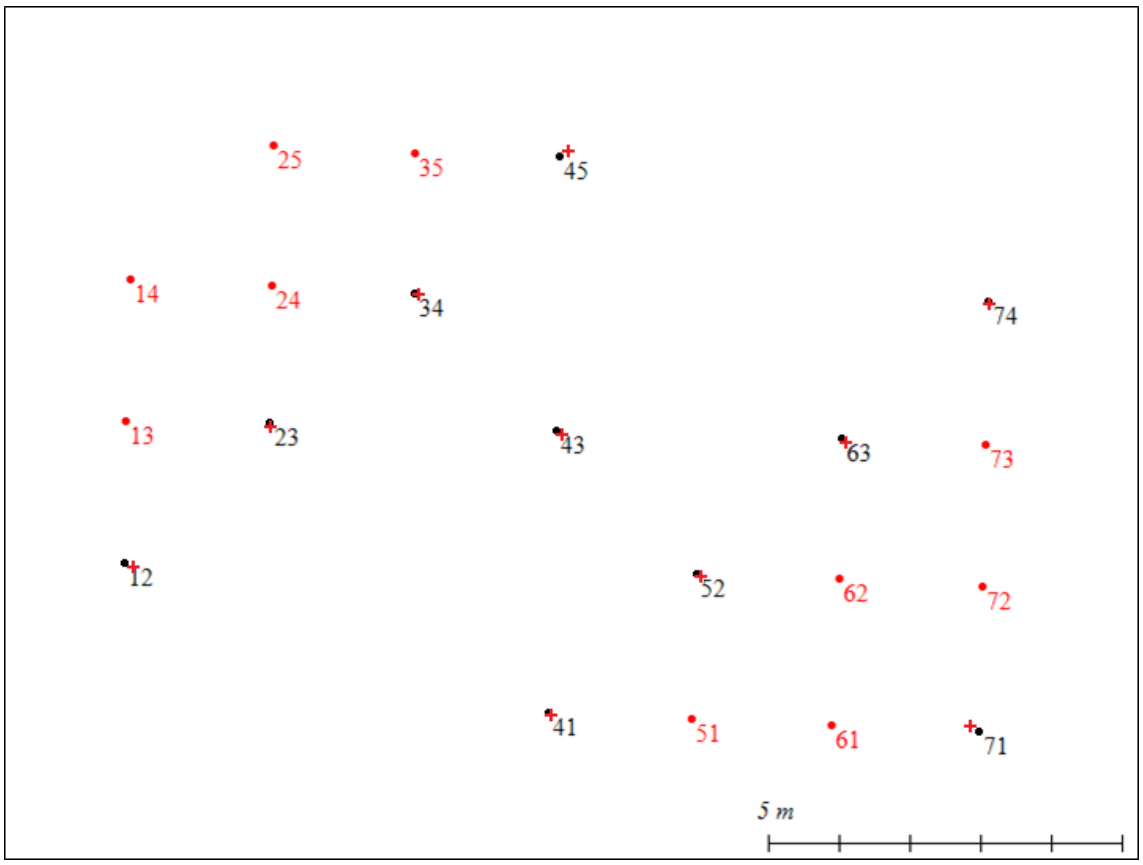

FIGURE 8. Multi-camera calibration: a) Camera 1 view; b) Camera 4 view; c) mapping of the calibration points in the real world. In **red**: the original points with known real-world positions; in **black**: the 'common points' and their true real-world positions; **red cross**: the estimated positions of the 'common points' in the real world.

DATASET II

Data collection set-up

The second location was a real traffic intersection (FIGURE 9). It was filmed with a camera installed on the top of a water tower. An additional photo image was taken from a building on the opposite side of the intersection. The calibration points were limited to the actual landmarks, such as sharp corners of the road markings. The calibration point position was measured with a high-precision GNSS[1] receiver, providing accuracy for static points of 1.5–2 cm. Most of the measured points could also be found in a satellite image from Google Maps.

A car, equipped with the same type of GNSS receiver, drove through the intersection several times, performing different manoeuvres. The position was saved with a frequency of 5 Hz; however, the accuracy of the measurement was affected by the movement and short time for each measurement, and this varied from 5 to 70 cm (rms). Only measurements with an accuracy below 30 cm were used.

[1] Leica GX1230 GG, http://www.leica-geosystems.com/.

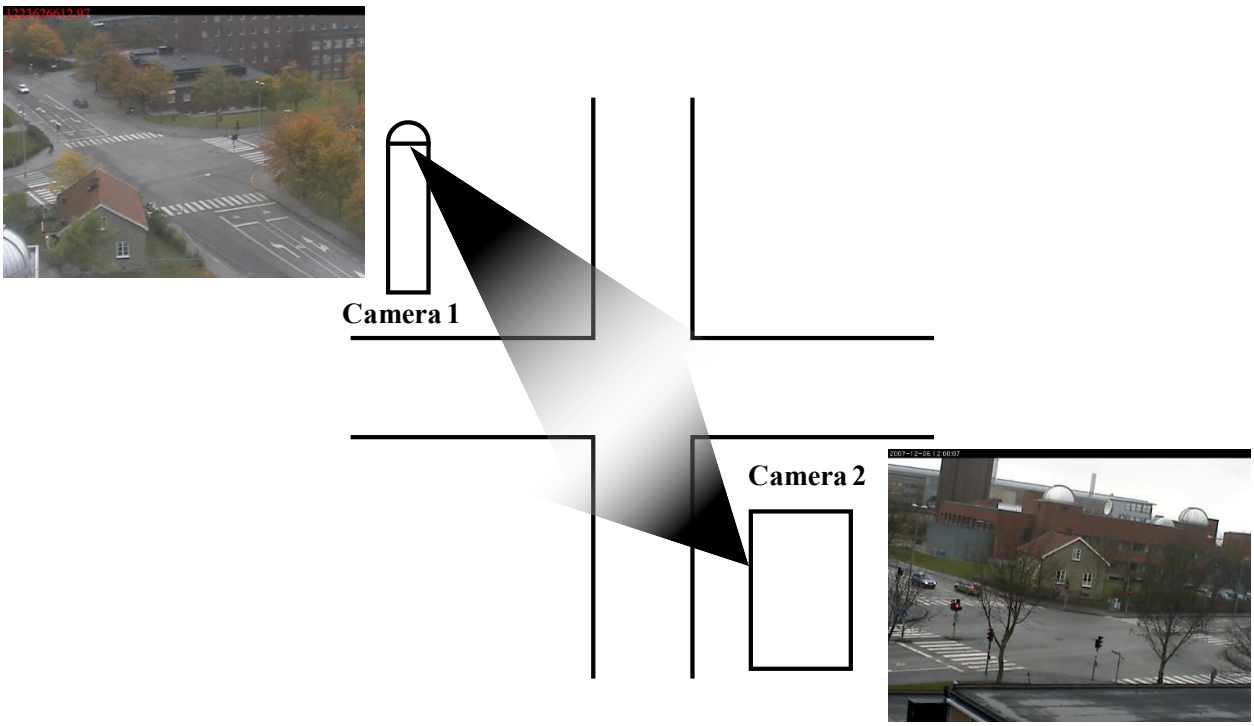

FIGURE 9. Camera set-up for Dataset II

Experiment 4.

In this experiment, we tested how well the trajectories of road users extracted from video (with different calibration models) fit the trajectories obtained from the GNSS tool. To extract the trajectory of a road user, a software tool, T-Analyst, was used [15]. This tool allows the user to browse a video frame by frame and to set a pre-defined wire-frame model so that it fits the road user in the image (FIGURE 10). The parameters of the wire-frame model were based exactly on the measurements of the car used in the experiment.

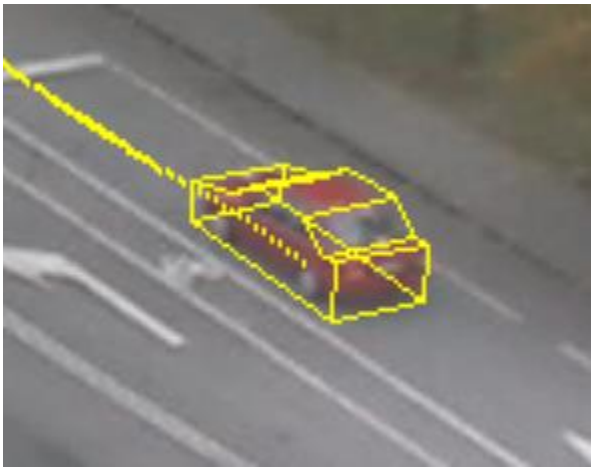

FIGURE 10. Wire-frame model

The following calibration scenarios were tested:

- All available calibration points with measured world co-ordinates used (FIGURE 11);

- Few poorly located points with world co-ordinates taken from a Google Maps satellite image (FIGURE 12);
- Multi-camera set-up calibration according to algorithm described in Experiment 3. The initial calibration of both cameras was done with few and unfavourably located points and the world co-ordinates taken from a satellite image (FIGURE 13).

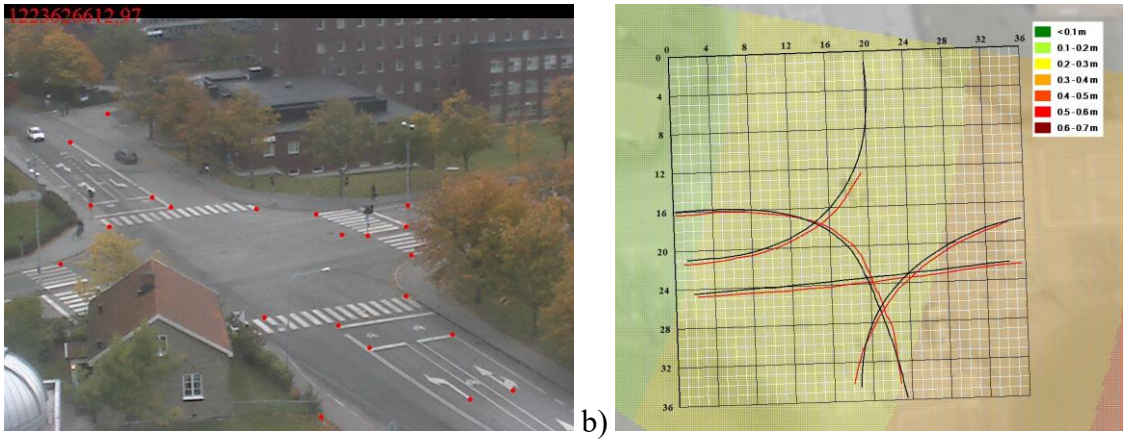

a) b)

FIGURE 11. Calibration based on measured 3D points: a) calibration points; b) trajectories obtained from GNSS (black) and video (red). The colours in the background show the 'price' of an image pixel error in world distance units; it should be considered that as the 'price' increases, a lower accuracy of the video-based trajectory points should be expected.

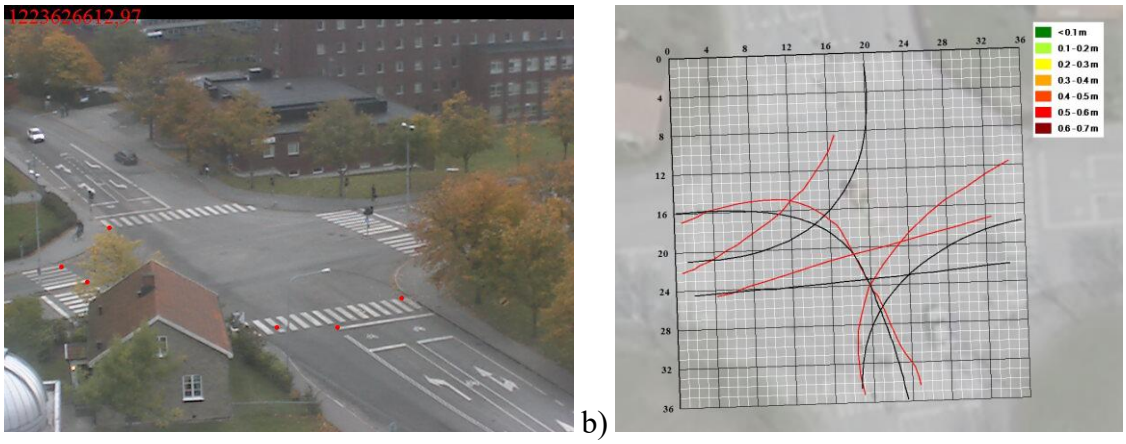

a) b)

FIGURE 12. Calibration based on few points and world co-ordinates obtained from a satellite image: a) calibration points; b) trajectories from GNSS (black) and video (red).

a) 

b) 

c) 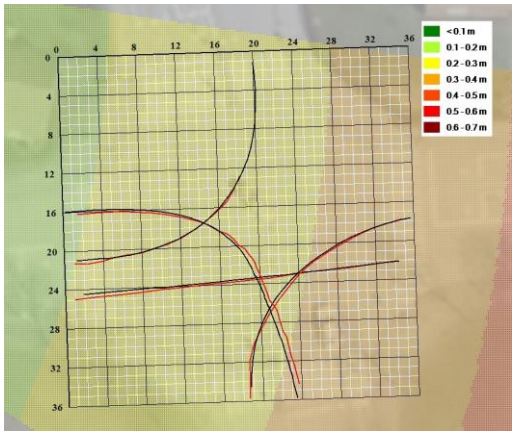

FIGURE 13. Multi-camera calibration: a), b) points used for initial calibration (red) and 'common points' without known world co-ordinates (green); c) trajectories obtained from GNSS (black) and video (red).

Not surprisingly, calibration based on few points (second scenario) failed completely. However, when the same set of points was used together with another camera view in a multi-camera calibration, highly satisfactory results were obtained. In fact, it appears that the multi-camera calibration provides a better fit with the GNNS data compared to the calibration based on accurately measured points in the first scenario. An explanation might be that the availability of the height data for points in the first scenario allows for an estimation of the correct horizontal plane on which road users can move, while the actual road surface was not horizontal. The point co-ordinates obtained from the satellite image lack height data; thus, the estimated zero-plane is not horizontal, and it is more adjusted to the actual road surface.

Generally, the assumption that road users are moving on the zero-plane might result in inaccuracies if the studied area is not flat (for example, if one of the intersection legs had a more acute incline compared to the rest of the intersection). This becomes even more probable if a larger area is studied (e.g. covered with several cameras). To compensate, it might be necessary to create a model of the road surface (for example, by interpolating the heights of the measured points); instead of always assuming that road users travel on the zero-plane, the actual height calculated by the surface model can be used.

CONCLUSIONS

Carefully choosing calibration points appears highly crucial to the quality of the final calibration model. Ideally, these points should cover evenly the entire camera image, but their locations around the studied area (e.g. zebra markings around an intersection) might still be a reasonable compromise.

Camera height affects the accuracy of the measurements, but to a lesser extent than calibration point selection.

Inaccurate world co-ordinates of the calibration points (e.g. taken from a blurry satellite image) result easily in an inadequate calibration model. Additional visual control of the obtained calibration (e.g. by drawing a grid on the zero-plane) is highly recommended.

The use of several camera views with 'common points' may greatly improve the calibration of each single camera. The additional camera views do not necessarily require another video camera installation, and they can be taken simply with a mobile phone or a photo camera, thus minimising the additional work required.

The introduction of a road surface height model might be an additional step towards improving the accuracy of measurements from videos. This might be particularly important in the case of a large study area in which significant height variations are possible; thus, the assumption that road users move on the zero-plane might be insufficient.

In this study, we have not investigated the temporal aspect of the measurements from videos (for example, the accuracy of speed and acceleration calculated based on the positions measured from a video). This aspect should be addressed in future research.

ACKNOWLEDGMENTS AND DISCLAIMER

This work has received funding from the European Union's Horizon 2020 research and innovation programme under grant agreement No 635895. Some data were collected in a project financed by Vinnova, Sweden's innovation agency.

This publication reflects only the authors' views. The European Commission and Vinnova are not responsible for any use of the information it contains.

REFERENCES

[1] Laureshyn, A., de Goede, M., Saunier, N. and Fyhri, A. Cross-comparison of three surrogate safety methods to diagnose cyclist safety problems at intersections in Norway. *Accident Analysis & Prevention*, No. 105, 2017, pp. 10-20. http://dx.doi.org/10.1016/j.aap.2016.04.035.

[2] Saunier, N., Sayed, T. and Ismail, K. Large scale automated analysis of vehicle interactions and collisions. *Transportation Research Record*, No. 2147, 2010, pp. 42-50. http://dx.doi.org/10.3141/2147-06.

[3] Madsen, T. and Lahrmann, H. Comparison of five bicycle facility designs in signalized intersections using traffic conflict studies. *Transportation Research Part F: Traffic Psychology and Behaviour*, No. 46 (Part B), 2017, pp. 438-450. https://doi.org/10.1016/j.trf.2016.05.008.

[4] van der Horst, A.R.A., Thierry, M.C., Vet, J.M. and Rahman, A.F. An evaluation of speed management measures in Bangladesh based upon alternative accident recording, speed measurements, and DOCTOR traffic conflict observations. *Transportation Research Part F*, No. 46, 2017, pp. 390-403. http://dx.doi.org/10.1016/j.trf.2016.05.006.
[5] St-Aubin, P., Miranda-Moreno, L. and Saunier, N. A surrogate safety analysis at protected freeway ramps using cross-sectional and before-after video data. *91st TRB Annual Meeting*, Washington DC, USA, 2012.
[6] Polders, E., Cornu, J., De Ceunynck, T., Daniels, S., Brijs, K., Brijs, T., Hermans, E. and Wets, G. Drivers′ behavioral responses to combined speed and red light cameras. *Accident Analysis & Prevention*, No. 81, 2015, pp. 153-166. http://dx.doi.org/10.1016/j.aap.2015.05.006.
[7] De Ceunynck, T., Dorleman, B., Daniels, S., Laureshyn, A., Brijs, T., Hermans, E. and Wets, G. Sharing is (s)caring? Interactions between buses and bicyclists on bus lanes shared with bicyclists. *Transportation Research Part F: Traffic Psychology and Behaviour*, No. 47, 2017, pp. 301-315. http://dx.doi.org/10.1016/j.trf.2016.09.028.
[8] Archer, J.: 'Indicators for traffic safety assessment and prediction and their application in micro-simulation modelling: a study of urban and suburban intersections'. Doctoral thesis, Royal Institute of Technology, Stockholm, Department of Infrastructure, 2005.
[9] Huang, F., Liu, P., Yu, H. and Wang, W. Identifying if VISSIM simulation model and SSAM provide reasonable estimates for field measured traffic conflicts at signalized intersections. *Accident Analysis & Prevention*, No. 50, 2013, pp. 1014-1024. http://dx.doi.org/10.1016/j.aap.2012.08.018.
[10] Wu, J., Radwan, E. and Abou-Senna, H. Determine if VISSIM and SSAM could estimate pedestrian-vehicle conflicts at signalized intersections. *Journal of Transportation Safety & Security*, 2017. http://dx.doi.org/10.1080/19439962.2017.1333181.
[11] Heikkilä, J. and Silven, O. A four-step camera calibration procedure with implicit image correction. *IEEE Conference on Computer Vision and Pattern Recognition*, 1997.
[12] Tsai, R.Y. A Versatile Camera Calibration Technique for High-Accuracy 3D Machine Vision Metrology Using Off-the-Shelf TV Cameras and Lenses. *IEEE Journal of Robotics and Automation*, No. RA-3 (4), 1987, pp. 323-344. https://doi.org/10.1109/JRA.1987.1087109.
[13] Zhang, Z. A flexible new technique for camera calibration. *IEEE Transactions on Pattern Analysis and Machine Intelligence*, No. 22 (11), 2000, pp. 1330-1334.
[14] Klein, L.A. "ITS sensors and architectures for traffic management and connected vehicles" CRC Press, Taylor & Francis group, Boca Raton, 2018. https://doi.org/10.1201/9781315206905.
[15] T-Analyst. Software for semi-automated video processing (Acc. 04 Apr 2017): www.tft.lth.se/software.
[16] Willson, R. Tsai Code implementation (currently not accessible) (Acc. 15 Jan 2014): http://www-2.cs.cmu.edu/afs/cs.cmu.edu/user/rgw/www/TsaiCode.html.